PCCP

Accepted Manuscript

ROYAL SOCIETY OF CHEMISTRY

www.rsc.org/pccp

Tuning electronic properties of Ti-MoS_2 contact through introducing vacancy in monolayer MoS_2

Li-ping Feng*, Jie Su, Da-peng Li, Zheng-tang Liu

State Key Lab of Solidification Processing, College of Materials Science and Engineering, Northwestern Polytechnical University, Xi'an, Shaanxi, 710072, People's Republic of China

ABSTRACT: Effect of vacancy in Monolayer MoS_2 on electronic properties of Ti-MoS_2 top contact has been investigated using first-principles calculations. Mo-vacancy is easier to form than S-vacancy in Ti-MoS_2 top contact, especially under oxidation conditions. Mo-vacancy eliminates the Schottky barrier of Ti-MoS_2 top contact, and S-vacancy reduces the Schottky barrier from 0.28 to 0.15 eV. Mo-vacancy is beneficial to get high quality *p*-type Ti-MoS_2 top contact, whereas S-vacancy is favorable to achieve high quality *n*-type Ti-MoS_2 top contact. Moreover, defective Ti-MoS_2 top contacts have stronger dipole layers, higher potential step and more transferred charges than perfect one. Electronic properties of Ti-MoS_2 top contacts can be tuned by intrinsic vacancy in monolayer MoS_2. Our findings provide important insights into future designing and fabrication of novel nanoelectronic devices with monolayer MoS_2.

KEYWORDS: Density functional theory; Monolayer MoS_2; Vacancy; Electronic properties

Monolayer transition-metal dichalcogenides (mTMD) semiconductors are considered promising candidates for channel materials in next-generation nanoelectronic devices. Monolayer molybdenum disulifide (MoS_2), one of two-dimensional mTMD semiconducting crystal, has drawn tremendous attention due to its atomically thickness of ~7 Å/layer [1], considerable band gap of 1.8 eV [2], planar nature, distinctive electronic and optical properties [3, 4]. Most recently, field-effect transistors (FETs) with monolayer MoS_2 as channel material show higher current on/off ratios and lower power consumption than classical transistors [5]. New phototransistor based on monolayer MoS_2 has been demonstrated to have a better photoresponsivity as compared with the graphene-based device [6]. Moreover, monolayer MoS_2 has been used to construct FET based biosensors, which exhibit highly advantageous over all other

* Corresponding author. Tel.: +86 29 88488013; fax: +86 29 88492642.
E-mail: lpfeng@nwpu.edu.cn (Dr. L. P. FENG)

nanomaterial-based FET biosensors [7].

Metal contacts to monolayer MoS_2 is a critical issue for its transistor applications [8, 9]. Understanding the physical nature of metal-MoS_2 contact is important for controlling electronic transparency and contact resistance, which are limiting factors for device performance [10]. Therefore, many studies have been performed to research the electronic characteristics of metal-MoS_2 contacts [8, 11-14]. Recently, transition metal Ti has obtained more attention because it has d orbitals, which may favorably mix with the Mo 4d states and enlarge the orbital overlaps. Popov et al. [12] have found that Ti is more efficient than the common contact Au metal for electron injection into monolayer MoS_2. Moreover, many experiments and calculations have shown that Ti-MoS_2 contact has an Ohmic character with lower Schottky barrier than other In-, Al-, Au-, and Pd-MoS_2 contacts [8, 11, 13]. Therefore, Ti has been proposed as a promising alternative contact metal to monolayer MoS_2.

Vacancy defects have been found to exist in monolayer MoS_2 when monolayer MoS_2 was obtained through many methods [15]. Several literatures have reported that the structural, electronic, and optical properties of monolayer MoS_2 depend greatly on its intrinsic vacancies [16-18]. It should be noted that vacancy defects in monolayer MoS_2 not only influence the properties of monolayer MoS_2 but also affect the interfacial and electrical properties of metal-MoS_2 contacts. However, to the best of our knowledge, effects of vacancies in monolayer MoS_2 on electronic structure and electronic properties of Ti-MoS_2 contact are not well understood yet. As we know, the knowledge of electronic properties of Ti-MoS_2 contact is very important for its practical applications as well as for the designing and analyzing of optoelectronic devices. Therefore, in this work, electronic properties of Ti-MoS_2 top contacts with vacancy in monolayer MoS_2 have been investigated using first-principles calculations.

In the present calculations, the generalized gradient approximation (GGA) with Perdew-Burke-Ernzerhof (PBE) functional as implemented in CASTEP [19] is adopted to describe electron exchange and correlation. In order to consider the van der Waals force in TMD materials, DFT-D2 approach is used, where

a semi-empirical dispersion potential described by a simple pair-wise force field is added to the conventional Kohn-Sham DFT energy [20]. The ionic cores were represented by ultrasoft pseudopotential for Ti, Mo and S atoms. The Ti 3d4s, Mo 4d5s and S 3s3p electrons were regarded as valence electrons. Ti-MoS_2 top contact was modeled by a supercell slab, which is periodic in the *x* and *y* directions and separated by 20 Å vacuum in the *z* direction to minimize the interactions between adjacent image cells. The supercell slab of Ti-MoS_2 top contact contains 4×4 unit cells of monolayer MoS_2 and the close-packed surface of Ti (001) extending to the 6th layer. Fig. 1(a) shows schematic of a monolayer MoS_2 FET and Fig. 1(b) presents the side view of supercell geometry of perfect Ti-MoS_2 top contact. Geometries of defective Ti-MoS_2 top contacts with Mo- and S-vacancy are presented in Fig. 1(c) and (d), respectively. After extensive convergence analysis, the plane-wave cutoff energy was set to be 720 eV. The number of k points in the unit cell was set to be 200 (10×10×2) for monolayer MoS_2 and 1000 (10×10×10) for Ti-MoS_2 contact, where the self-consistent convergence of the total energy is 1.0×10^{-6} eV/atom. Under the calculational conditions, monolayer MoS_2 shows direct band gap of 1.8 eV, which is consistent with results obtained by experiments [2].

Formation energies of S- and Mo-vacancy in Ti-MoS_2 contacts were calculated. Fig. 2 shows the formation energies of intrinsic vacancy as a function of the sulfur chemical potential ($\Delta\mu_s$). It can be seen that the formation energy of Mo-vacancy in Ti-MoS_2 top contact increases monotonously as $\Delta\mu_s$ varies from oxidization limit to reduction limit, implying that Ti-MoS_2 top contact with Mo-vacancy is more stable under oxidization conditions. Nevertheless, the formation energy of S-vacancy in Ti-MoS_2 top contact shows an opposite trend compared with that of Mo-vacancy in Ti-MoS_2 top contact. The variations of the formation energies of Mo- and S-vacancy in Ti-MoS_2 top contact are consistent with those of Mo- and S-vacancy in monolayer MoS_2 [16]. Moreover, in Fig. 2, the formation energy of Mo-vacancy maintains negative whereas that of S-vacancy keeps positive, indicating Mo-vacancy creation is easier than S-vacancy in Ti-MoS_2 top contact.

Partial density of states (PDOS) of all atomic species of perfect and defective Ti-MoS_2 top contacts are

shown in Fig. 3, and compared with those of intrinsic monolayer MoS_2. Fig. 3(a) presents the PDOS of intrinsic monolayer MoS_2. It can be seen that the top of valence bands and the bottom of conduction bands of monolayer MoS_2 are dominated by the hybridization of anti-bonding and bonding between Mo 4*d* and S 3*p* states. The PDOS of perfect Ti-MoS_2 top contact is shown in Fig. 3(b). Upon contacting to Ti, both Mo 4*d* and S 3*p* states of monolayer MoS_2 shift downward and spread all over the original band gap of intrinsic monolayer MoS_2. Some S 3*p* states hybridize with Ti 3*d* states near the Fermi level (E_F), suggesting the formation of Ti-S chemical bonding at the interface of Ti-MoS_2 top contact. Besides, a large overlap between Mo 4*d* and Ti 3*d* states is found near the E_F, indicating metallic character of perfect Ti-MoS_2 top contact. The E_F of perfect Ti-MoS_2 top contact is shifted towards the bottom of original conduction bands of monolayer MoS_2, showing that perfect Ti-MoS_2 top contact is doped *n*-type by Ti. The valence bands maximum (E_{VBM}) of intrinsic monolayer MoS_2 can be determined by the following equation [21, 22]:

$$E_{VBM}(\text{intrinsic})=E_{VBM}(\text{interface})-V_{av}(\text{interface})+V_{av}(\text{intrinsic}) \quad (1)$$

where E_{VBM}(intrinsic) and E_{VBM}(interface) are the E_{VBM} of intrinsic monolayer MoS_2 and monolayer MoS_2 in Ti-MoS_2 top contact, respectively. V_{av}(intrinsic) and V_{av}(interface) represent the average potential of intrinsic monolayer MoS_2 and monolayer MoS_2 in Ti-MoS_2 top contact, respectively. As a result, the borders of the E_{CBM} and E_{VBM} of intrinsic monolayer MoS_2 are marked as vertical dash lines in the PDOS of Ti-MoS_2 top-contacts, as shown in Fig. 3. The dot line in Fig. 3 represents the E_F of Ti-MoS_2 top contact. According to the previous studies [8, 23], the *n*-type (*p*-type) Schottky barrier is the difference between the E_{CBM} (the E_{VBM}) of intrinsic monolayer MoS_2 and the E_F of the monolayer MoS_2 in Ti-MoS_2 top contact. Hence, in Fig. 3(b), Schottky barrier of perfect Ti-MoS_2 top contact is about 0.28 eV, which is in good agreement with other calculational and experimental data [12, 24]. Moreover, high PDOS surround the E_F implies the formation of Ohmic contact between Ti metal and monolayer MoS_2, which is consistent with previous theoretical and experimental reports for Ti-MoS_2 top contact [8, 14, 24].

Fig. 3(c) shows the PDOS of Ti-MoS_2 top contact with Mo vacancy. It is clear that interactions between

S 3*p* and Ti 3*d* states become stronger and that overlaps between Mo 4*d* and Ti 3*d* states get larger compared with those of perfect one. On one hand, the dangling bonding of S atoms surrounding Mo-vacancy may rebind with Ti to strength the Ti-S bonding. On the other hand, the decrease of physical distance between Ti metal and monolayer MoS_2 enhance the overlap of their *d* states. Thus, higher and wider PDOS, consist of Mo 4*d* and S 3*p* states, spread all over the original band gap of monolayer MoS_2, implying that Mo-vacancy further improves Ohmic character and metallic behavior of the Ti-MoS_2 top contact. The Schottky barrier of Ti-MoS_2 top contact with Mo-vacancy is vanished, indicating higher electron injection efficiency. Moreover, some peaks of PDOS appear near the top of original valence bands of monolayer MoS_2, suggesting that Mo-vacancy in monolayer MoS_2 is suitable to get *p*-type Ti-MoS_2 top contact. Fig. 3(d) presents the PDOS of Ti-MoS_2 top contact with S vacancy. It is obvious that the PDOS of the defective Ti-MoS_2 top contact are higher and wider than those of perfect one. The Schottky barrier of 0.15 eV is found for Ti-MoS_2 top contact with S-vacancy, which is smaller than that of perfect one. Furthermore, some high peaks of PDOS, dominated by Mo 4*d* states with small admixture of S 3*p* states, are observed near the bottom of original conduction bands of monolayer MoS_2, indicating that S-vacancy brings about *n*-type Ti-MoS_2 top contact.

To illustrate the nature of charge transfer at the interface of contacts, electron difference density and schematic of band structure of Ti-MoS_2 top contacts without defect, with Mo-vacancy, and with S-vacancy are shown in Figs. 4(a-c), respectively. In Fig. 4(a), several charge transferred oscillations are observed on electron difference density near the interface of perfect Ti-MoS_2 top contact, which indicates the formation of interfacial dipole layers [25]. The dipole layers result in a potential step, ΔV, in the potential energy perpendicular to the interface [25]. Electrons are piled in the dipole layer on the surface of Ti metal, implying depletion is close to the surface of monolayer MoS_2 because the work function of Ti is larger than that of monolayer MoS_2 [8, 26]. As to chemisorption interface, the strong chemical interactions between these dipole layers can induce buckled surfaces in the interface and further increase the potential step [23], leading to the Schottky barrier of perfect Ti-MoS_2 top contact lower than the difference of work function between pristine

metal Ti and intrinsic monolayer MoS_2. After introduction of Mo vacancy in monolayer MoS_2, the electrons transferred from monolayer MoS_2 to Ti are increased. Therefore, more positive charges are piled on the surface of monolayer MoS_2 as well as stronger dipole layers are formed at the interface, as exhibited in Fig. 4(b). The drastic reordering charges lead to the decrease of the E_F of monolayer MoS_2. Moreover, higher peaks are observed for electron difference density at the interface of Ti-MoS_2 top contact with Mo-vacancy, indicating the strengthened chemical interactions between Ti metal and monolayer MoS_2. Due to the larger charge redistribution and the stronger chemical interactions, the potential step of Ti-MoS_2 top contact with Mo-vacancy becomes higher, which brings about the E_F of the contact descending into the original valence bands of monolayer MoS_2. Hence, the Schottky barrier of Ti-MoS_2 top contact with Mo-vacancy is disappeared. In Fig. 4(c), Ti-MoS_2 top contact with S-vacancy also has more electrons transferred from monolayer MoS_2 to metal Ti than perfect one. Thus, many negative charges are localized on the surface of Ti metal, and then the work function of Ti is decreased [27], but the value is still higher than that of monolayer MoS_2 with S-vacancy. So the schematic of band structure of the defective Ti-MoS_2 contact is similar to that of perfect one. Nevertheless, the peaks of electron difference density at the interface of the defective Ti-MoS_2 contact are a little higher than those of perfect one, suggesting stronger chemical interactions and a little larger potential step. Simultaneously, S-vacancy causes the increase of the E_F of monolayer MoS_2 [18]. These results lead to a narrow Schottky barrier for Ti-MoS_2 top contact with S-vacancy.

In summary, we investigate the electronic properties of perfect and defective Ti-MoS_2 top contacts using first-principles calculations. Results show that the electronic properties of Ti-MoS_2 top contacts can be tuned by intrinsic vacancy in monolayer MoS_2. Upon Mo- or S-vacancy forming in monolayer MoS_2, higher and wider PDOS as well as lower Schottky barrier are observed for defective Ti-MoS_2 top contacts. Additionally, more transferred charges, stronger dipole layers and higher potential step are found for defective Ti-MoS_2 top contacts. Mo-vacancy in monolayer MoS_2 results in *p*-type Ti-MoS_2 top contact, whereas S-vacancy in monolayer MoS_2 brings about *n*-type Ti-MoS_2 top contact.

AUTHOR INFORMATION

Corresponding Author

*E-mail: lpfeng@nwpu.edu.cn

Notes

The authors declare no competing financial interest.

ACKNOWLEDGMENTS

We acknowledge the National Natural Science Foundation of China under grant No. 61376091, the National Aerospace Science Foundation of China under grant No. 2014ZF53070, and the Fundamental Research Funds for the Central Universities under grant No. 3102014JCQ01033.

REFERENCES

[1] M. M. Benameur, B. Radisavljevic, J. S. Heron, H. Berger, A. Kis. *Nanotechnol.* 2011, **22**, 125706.

[2] K. F. Mak, C. Lee, J. Hone, J. Shan, T. F. Heinz. *Phys. Rev. Lett*. 2010, **105**, 136805.

[3] K. F. Mak, K. He, J. Shan, T. F. Heinz. *Nat. Nanotechnol.* 2012, **7**, 494-498.

[4] S. W. Han, H. Kwon, S. K. Kim, S. Ryu, W. S. Yun, D. H. Kim, et al. *Phys. Rev. B* 2011, **84**, 045409.

[5] B. Radisavljevic, A. Radenovic, J. Brivio, V. Giacometti, A. Kis. *Nat. Nanotechnol*. 2011, **6**, 147-150.

[6] Z. Yin, H. Li, H. Li, L. Jiang, Y. Shi, Y. Sun, et al. *ACS Nano* 2012, **6**, 74-80.

[7] D. Sarkar, W. Liu, X. Xie, A. Anselmo, S. Mitragotri, K. Banerjee. *ACS Nano* 2014, **8**, 3992-4003.

[8] J. Kang, W. Liu, D. Sarkar, D. Jena, K. Banerjee. *Phys. Rev. X* 2014, **4**, 031005.

[9] J. Kang, W. Liu, K. Banerjee. *Appl. Phys. Lett*. 2014, **104**, 093106.

[10] M. S. Fuhrer, J. Hone. *Nat. nanotechnol.*, 2013, **8**, 146-147.

[11] J. Kang, D. Sarkar, W. Liu, D. Jena, K. Banerjee. *IEEE International Electron Devices Meeting*. 2012, 407-410.

[12] I. Popov, G. Seifert, D. Tomanek. *Phys. Rev. Lett*. 2012, **108**, 156802.

[13] W. Liu, J. Kang, D. Sarkar, Y. Khatami, D. Jena, K. Banerjee. *Nano Lett.*, 2013, **13**, 1983-1990.

[14] S. Das, H. Y. Chen, A. V. Penumatcha, J. Appenzeller. *Nano Lett.*, 2012, **13**, 100-105.

[15] S. McDonnell, R. Addou, C. Buie, R. M. Wallace, C. L. Hinkle. *ACS Nano* 2014, **8**, 2880-2888.

[16] L. P. Feng, J. Su, S. Chen, Z. T. Liu. *Mater. Chem. Phys*. 2014, **148**, 5-9.

[17] C. Ataca, H. Sahin, E. Akturk, S. Ciraci. *J. Phys. Chem. C* 2011, **115**, 3934-3941.

[18] L. P. Feng, J. Su, Z. T. Liu. *J. Alloy Compd.* 2014, **613**, 122-127.

[19] M. D. Segall, P. J. D. Lindan, M. J. Probert, C. J. Pickard, P. J. Hasnip, S. J. Clark, M. C. Payne. *J. Phys.: Condens. Matter.* 2002, **14**, 2717-2744.

[20] T. Bučko, J. Hafner, S. Lebegue, J. G. Angyán. *J. Phys. Chem. A* 2010, **114**, 11814-11824.

[21] A. Garcia and J. E. Northrup. *Phys. Rev. Lett*. 1995, **74**, 1131.

[22] S. Poykko, M. J. Puska, and R. M. Nieminen. *Phys. Rev. B* 1996, **53**, 3813.

[23] M. Bokdam, G. Brocks, M. I. Katsnelson, and P. J. Kelly. 2014, arXiv:1401.6440v2

[24] J. Y. Kwak, J. Hwang, B. Calderon, H. Alsalman, N. Munoz, B. Schutter, M. G. Spencer. *Nano Lett.*, 2014, **14**, 4511-4516.

[25] G. Giovannetti, P. A. Khomyakov, G. Brocks, V. M. Karpan, P. J. Kelly. *Phys. Rev. Lett.* 2008, **101**, 026803.

[26] P. A. Khomyakov, G. Giovannetti, P. C. Rusu, J. van den Brink, and P. J. Kelly. *Phys. Rev. B*, 2009, **79**, 195425.

[27] X. Ji, Y. Wang, Z. Yu. *Phys. Chem. Chem. Phys.*, 2014, **16**, 12327.

Figure captions list:

Fig. 1 (a) Schematic cross-sectional view of a monolayer MoS_2 FET. Dotted box represents Ti-MoS_2 top contact. (b) Side view of the perfect Ti-MoS_2 top contact. (c) Amplified sketch of Ti-MoS_2 top contact with Mo-vacancy. (d) Amplified sketch of Ti-MoS_2 top contact with S-vacancy. Color key is Ti=dark green, S=yellow, and Mo=green.

Fig. 2 Formation energies of individual vacancy defect versus the sulfur chemical potential ($\Delta\mu_s=\mu_s^0-\mu_s$), μ_s^0 is the total energies per atom of sulfur molecular. The formation energy is calculated for the whole 4×4 slabs of Ti-MoS_2 top contact.

Fig. 3 PDOS of adsorbate-free Ti slab and intrinsic monolayer MoS_2 (a), PDOS of perfect Ti-MoS_2 top contact (b), PDOS of defective Ti-MoS_2 top contact with Mo-vacancy (c), PDOS of defective Ti-MoS_2 top contact with S-vacancy (d). $\Phi_{SB,n}$ and $\Phi_{SB,p}$ are *n*- and *p*-type Schottky barrier, respectively.

Fig. 4 Charge redistribution and band structure of perfect Ti-MoS_2 contact (a), Ti-MoS_2 contact with Mo-vacancy (V_{Mo}) (b), Ti-MoS_2 contact with S-vacancy (V_S) (c). In each sub-figure ((a)-(c)), the left shows electron difference density along y projected on x-z plane coupling with the average value in the x-y planes normal to z-axis; the right shows schematic of band structure of Ti-MoS_2 top contact. E_{vac}, and E_F are the vacuum level and the Fermi level, respectively. W_M and ΔV represent the work function of adsorbate-free Ti and the potential step, respectively. "-" and "+" represent the electron and hole, respectively, their numbers mean the ability of charge redistribution.

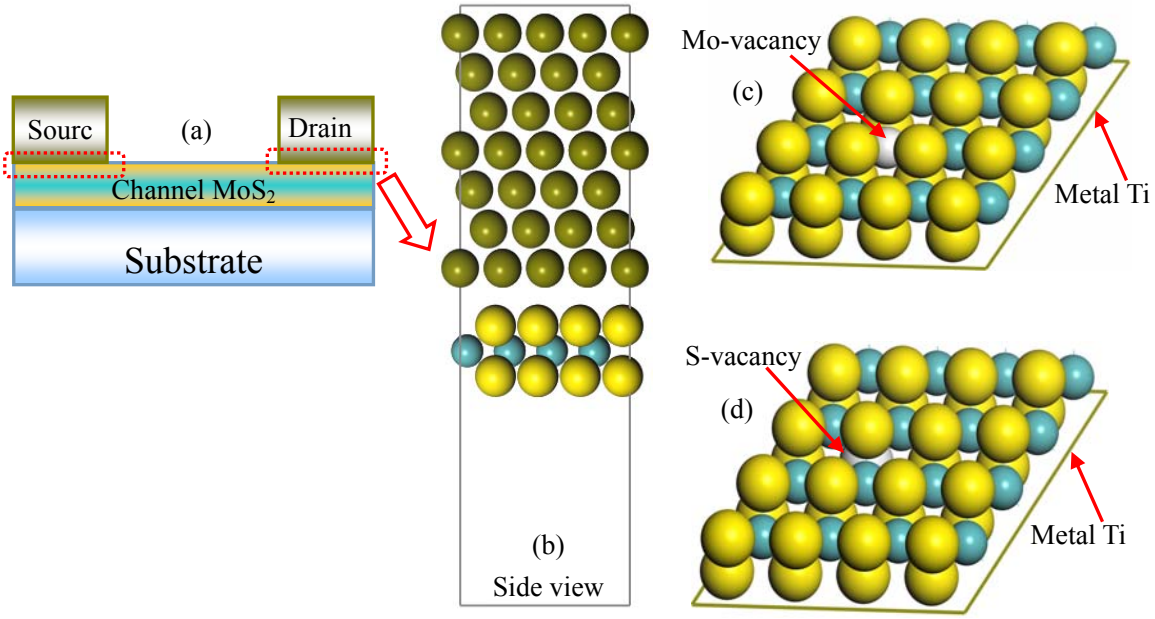

Fig. 1 (a) Schematic cross-sectional view of a monolayer MoS_2 FET. Dotted box represents Ti-MoS_2 top contact. (b) Side view of the perfect Ti-MoS_2 top contact. (c) Amplified sketch of Ti-MoS_2 top contact with Mo-vacancy. (d) Amplified sketch of Ti-MoS_2 top contact with S-vacancy. Color key is Ti=dark green, S=yellow, and Mo=green.

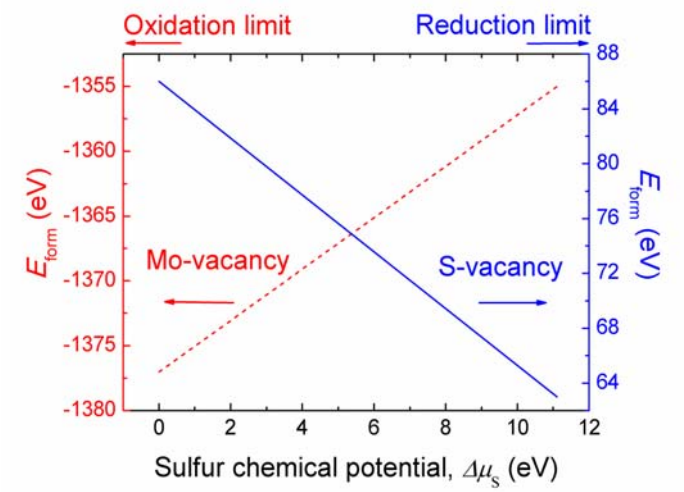

Fig. 2 Formation energies of individual vacancy defect versus the sulfur chemical potential ($\Delta\mu_S=\mu_S^0-\mu_S$), μ_S^0 is the total energies per atom of sulfur molecular. The formation energy is calculated for the whole 4×4 slabs of Ti-MoS_2 top contact.

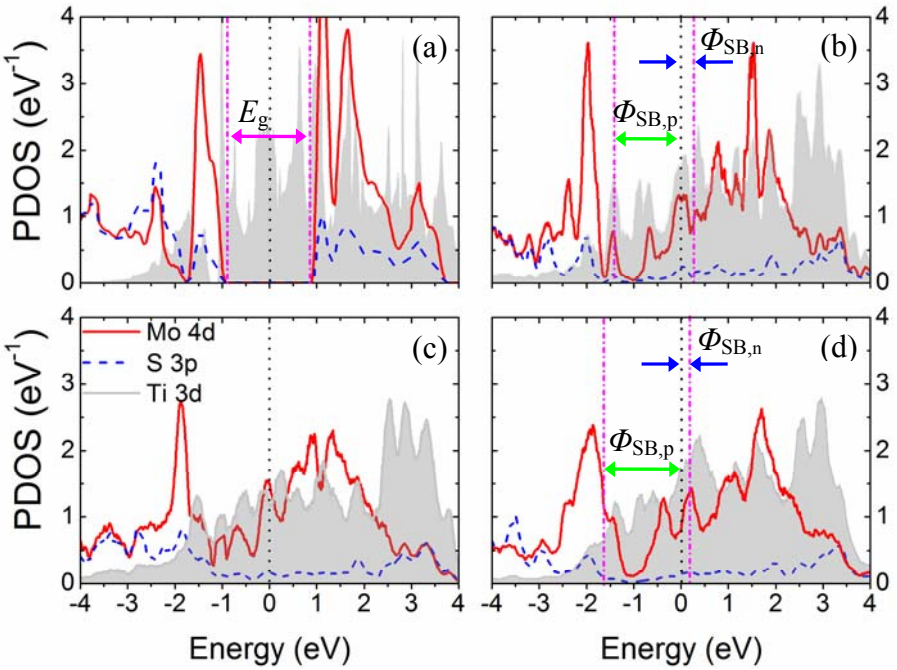

Fig. 3 PDOS of adsorbate-free Ti slab and intrinsic monolayer MoS_2 (a), PDOS of perfect Ti-MoS_2 top contact (b), PDOS of defective Ti-MoS_2 top contact with Mo-vacancy (c), PDOS of defective Ti-MoS_2 top contact with S-vacancy (d). $\Phi_{SB,n}$ and $\Phi_{SB,p}$ are *n*- and *p*-type Schottky barrier, respectively.

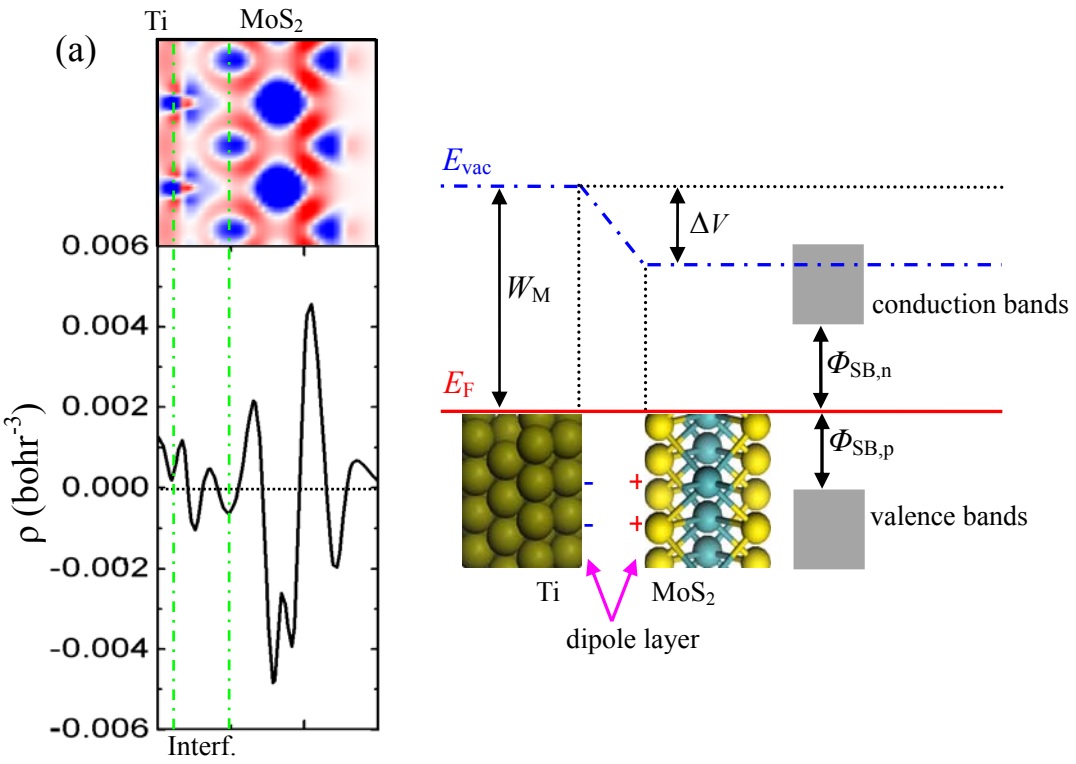

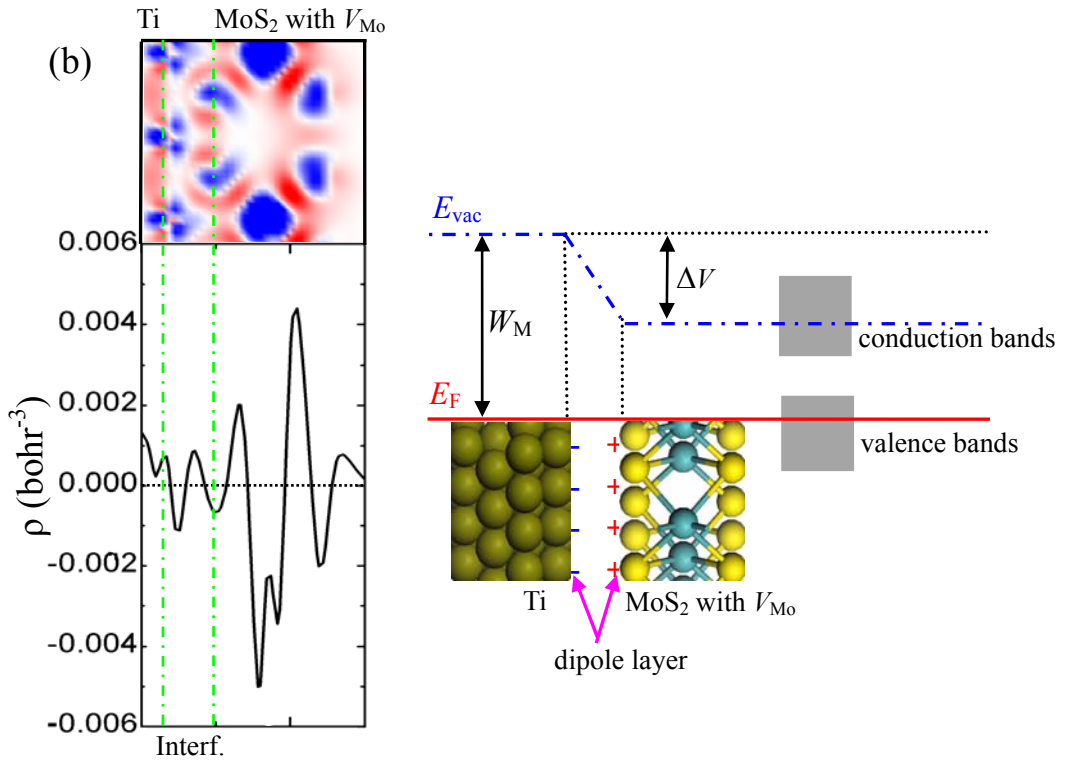

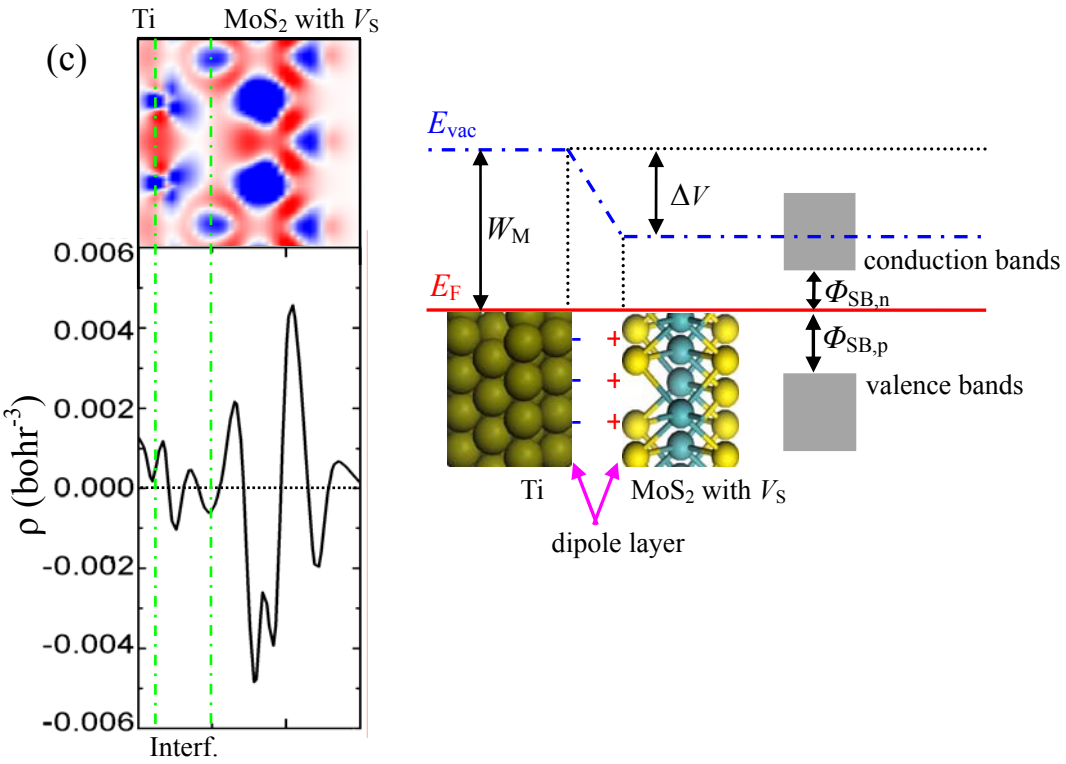

Fig. 4 Charge redistribution and band structure of perfect Ti-MoS_2 contact (a), Ti-MoS_2 contact with Mo-vacancy (V_{Mo}) (b), Ti-MoS_2 contact with S-vacancy (V_S) (c). In each sub-figure ((a)-(c)), the left shows electron difference density along y projected on x-z plane coupling with the average value in the x-y planes normal to z-axis; the right shows schematic of band structure of Ti-MoS_2 top contact. E_{vac}, and E_F are the vacuum level and the Fermi level, respectively. W_M and ΔV represent the work function of adsorbate-free Ti and the potential step, respectively. "-" and "+" represent the electron and hole, respectively, their numbers mean the ability of charge redistribution.